Deep–Sea Research II 180 (2020) 104819

Contents lists available at ScienceDirect

Deep-Sea Research Part II

journal homepage: http://www.elsevier.com/locate/dsr2

Biophysical models of persistent connectivity and barriers on the northern Mid-Atlantic Ridge

J.M. Yearsley [a,b,*], D.M. Salmanidou [a,b,c], J. Carlsson [a,b], D. Burns [a], C.L. Van Dover [d]

[a] School of Biology and Environmental Science, University College Dublin, Belfield, Dublin 4, Ireland
[b] UCD Earth Institute, University College Dublin, Belfield, Dublin 4, Ireland
[c] Department of Statistical Science, University College London, Gower Street, London, WC1E 6BT, United Kingdom
[d] Division of Marine Science and Conservation, Nicholas School of the Environment, Duke University, Beaufort, NC, 28516, USA

ARTICLE INFO

Keywords:
Deep-sea mining
ARGO probes
Biophysical models
Larval dispersal
Mid-atlantic ridge
Connectivity
Mathematical models
Biotic barriers
Dynamical oceanography
Marine parks

ABSTRACT

A precautionary approach to protecting biodiversity on mid-ocean ridges, while permitting seabed mining, is to design and implement a network of areas protected from the effects of mining. Such a network should capture representative populations of vent endemic fauna within regions of connectivity and across persistent barriers, but determining where such connectivity and barriers exist is challenging. A promising approach is to use biophysical modeling to infer the spatial scale of dispersal and the positions where breaks in hydrographic connectivity occur. We use results from a deep-sea biophysical model driven by data from the global array of Argo probes for depths of 1000 m to estimate biophysical connectivity among fragmented hydrothermal vent habitats along the Mid-Atlantic Ridge, from the equator northward to the Portuguese Exclusive Economic Zone surrounding the Azores. The spatial scale of dispersal varies along the ridge axis, with median dispersal distances for planktonic larval durations (PLDs) of 75 d ranging from 67 km to 304 km. This scale of dispersal leads to considerable opportunities for connectivity through mid-water dispersal. A stable pattern of five regions of biophysical connectivity was obtained for PLDs of 100 d or more. Connectivity barriers between these regions can persist even when planktonic larval duration extends beyond 200 d. For a 50 d PLD, one connectivity barrier coincides with the region of the genetic hybrid zone for northern and southern vent mussel species at the Broken Spur vent field. Additional barriers suggest potential for genetic differentiation that so far has not been detected for any taxon. The locations of persistent zones of connectivity and barriers to dispersal suggest that there may be multiple biogeographic subunits along the northern Mid-Atlantic Ridge that should be taken into account in planning for effective environmental management of human activities.

1. Introduction

Many deep-sea benthic invertebrate species have dispersive life-history stages that reside in the water column for durations of days to years (Hilário et al., 2015). As a consequence, three-dimensional structure and flow in the ocean interior are important in understanding processes that contribute to population connectivity or to persistent filters or barriers that might impose geographical constraints on gene flow of benthic taxa (Cowen and Sponaugle, 2009; Palumbi, 2003). Biophysical models of velocity fields and Lagrangian particle dispersal simulations provide insight into the scales at which circulation of the internal ocean may play a role in connecting or isolating benthic populations. This same insight into scales of larval transport mechanisms on a regional basis may also be useful in the design of networks of protected areas (Roberts, 1997), particularly when the design must be developed as a precautionary approach in the absence of comprehensive knowledge of larval dispersal and gene flow.

Recent biophysical modeling of larval dispersal in the deep ocean has relied on ocean general circulation models (e.g., Etter and Bower, 2015; McVeigh et al., 2017; Young et al., 2012). The mathematical equations in these models are based on physical properties of seawater (e.g., temperature, salinity) and of forcing functions (wind stress, surface buoyancy fluxes). They have the advantage of large areal and volumetric coverage, but they are dependent on low-resolution topographic data

Abbreviations: PLD, Planktonic larval duration; nMAR, northern Mid-Atlantic Ridge.

* Corresponding author. School of Biology and Environmental Science, University College Dublin, Belfield, Dublin 4, Ireland.
E-mail address: jon.yearsley@ucd.ie (J.M. Yearsley).

https://doi.org/10.1016/j.dsr2.2020.104819
Received 16 December 2019; Received in revised form 11 June 2020; Accepted 21 June 2020
Available online 26 July 2020

derived from satellite altimetry and have coarse vertical resolution as depth increases [e.g., to 1 data output every 500 m for depths from 2000 to 5500 m (Ross et al., 2016)]. Displacement vectors of a small fleet of profiling floats have been used to validate particle tracking models driven by a 3D ocean general circulation model that characterized dispersal of vent larvae in back-arc basins of the western Pacific (Mitarai et al., 2016). A complementary approach to ocean circulation models estimates Eulerian velocity fields of deep-ocean currents (Yearsley and Sigwart, 2011) from speeds and headings of the Argo fleet (Roemmich et al., 2009). These velocity fields represent aggregate horizontal displacements of drifting floats at a specified depth, geographical area, and time interval. While resolution of Argo vector data may, like ocean general circulation models, be coarse, Argo displacements are averaged from physical (not modelled) motions. Lagrangian larval particle tracking within Argo velocity fields can also be used to explore larval dispersal under specific conditions of release and planktonic larval duration (PLD).

In this study, we use biophysical models based on Argo float displacements to explore connectivity of benthic species endemic to patchy ecosystems with linear fragmentation, as is characteristic of taxa (Vrijenhoek, 2010) and communities (Mullineaux et al., 2018) endemic to hydrothermal vent habitats. We chose to focus on the northern Mid-Atlantic Ridge (nMAR), where area-based management tools (networks of 'no-mine' areas known as Areas of Particular Environmental Interest, or APEIs) may be part of a precautionary approach to protect marine ecosystems from the potential impacts of exploitation of polymetallic sulfide resources (Lodge et al., 2014). Most hydrothermal vents on the nMAR are at depths of 2000 to 4000 m, but entrainment in hydrothermal plumes (Kim et al., 1994), diapycnal mixing within the axial valley (Thurnherr et al., 2002), buoyancy imparted by lipid stores in eggs and embryos (Brooke and Young, 2009), long residence times in the water column (Ramirez-Llodra et al., 2000), and vertical migration behaviors (McVeigh et al., 2017) may facilitate displacement of larvae from the seabed into the midwater column. In this context, we note that maximum biomass of post-larval alvinocarid (vent) shrimp from along the Mid-Atlantic Ridge within our study area were netted from the shallowest depths sampled ("mid-water", 2000–2500 m) compared to samples from 2500-2750 m and 2750–3000 m (Herring and Dixon, 1998). Buoyancy of larvae will change during pelagic development (e.g., increasing as lipids are acquired by feeding larvae; decreasing as lipids are consumed by lecithotrophic larvae), making it likely that larval distributions in the water column, including where they may hit a density barrier to vertical movement, will be species- and life-history-stage specific.

The nominal drifting depth for Argo floats is the 1000-m isobath, which constrains models based on Argo data to ocean circulation experienced by larvae with mid-water distributions. Depth profiles of the mean Atlantic Meridional Overturning Circulation from ocean reanalyses shows coherence across broad depth regions (100's of meters) and a mixing layer depth consistently less than 1000 m (Danabasoglu et al., 2014; Jackson et al., 2019). We assume that there will be coherent flow for a zone that is considerably broader than a 1000-m isobath and thus refer to this as a "mid-water" zone. This mid-water circulation will be modified as currents interact with seabed topography, where, for example, there may be enhanced current speeds (average 6.9 km d^{-1}) in narrow portions of the axial valley of the nMAR (Keller et al., 1975).

The degree to which drifting Argo floats mimic larval dispersal is subject to the same caveats as those identified for ocean general circulation models, including dependence on distributions of reproductive benthic populations, larval behavior and vertical distributions, timing of larval release, and the role of episodic circulation events (Etter and Bower, 2015; Ross et al., 2016). And of course, vent-endemic larvae (or post-larvae) must ultimately reach a suitable benthic habitat with competency to settle and metamorphose, which may depend on a behavioral response to environmental cues, about which virtually nothing is known for vent animals (Rittschof et al., 1998). It remains challenging to map larval distributions in the field (Adams et al., 2012), forcing us to explore indirect methods of inferring connectivity and barriers to larval dispersal. In this study, we use mid-water velocity fields and Lagrangian particle dispersal simulations to i) test whether mid-water larval dispersal capacity varies along the nMAR for a given PLD, ii) explore the spatial scale of non-swimming larval dispersal, iii) calculate connectivity matrices for vent ecosystems on the nMAR under simulation conditions, and iv) consider how connectivity networks may inform design of a network of 'no-mine' APEIs on the nMAR.

2. Material and methods

2.1. Study area

The study area covers the northern Mid-Atlantic Ridge from the equator to 42°N, i.e., extending from the Romanche Fracture Zone to just south of the Azores (Fig. 1). Five computational windows (labelled A-E) were used to reduce the computational burden of the simulations (Fig. 1, Table 1). The computational windows were selected to ensure that the majority of simulated larval tracks would remain within a computational region during a simulation of 500-d dispersal.

2.2. Argo probe data

All Argo probe cycle data from 2000 to 2014 from a drifting depth between 800 and 1400 m (i.e., 1000 m: 41,527 probes; 1100 m: 64 probes; 1300 m: 1 probe) were downloaded from ftp://ftp.ifremer.fr/ifremer/argo/for the study area (Table 1, Fig. 2). The speeds of the Argo probes over one cycle (median cycle length: 10 d) had a similar distribution across all five computational windows (Fig. 2a). The distribution of probe speeds across all windows was well described by a Gamma distribution (Fig. 2b), consistent with Argo probe data from the

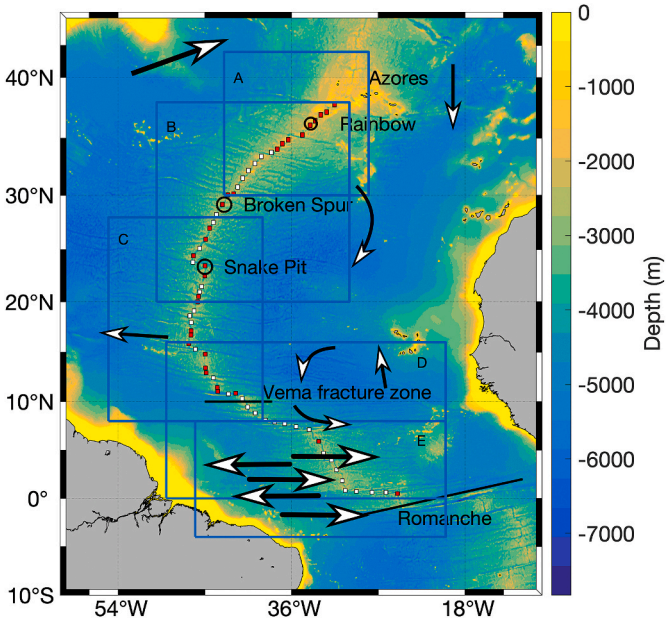

Fig. 1. The five computational windows (blue boxes labelled A-E, Table 1) and the 64 target boxes used to calculate connectivity (red squares: contain known vent sites; white squares only contain 'phantom' sites). Three named vent sites (Rainbow, Broken Spur, Snake Pit) are indicated (black circles) for orientation, as well as two fracture zones (Vema, Romanche, black lines) and the Azores Archipelago. Arrows are indicative of average currents at 1000 m depth, inferred from Argo probe trajectories (Colin de Verdière and Ollitrault, 2016). Strong zonal flows are shown around the equator. Each target box has dimensions of 0.4° longitude and 0.4° latitude. Bathymetry: NOAA ETOPO1.

Table 1
Bounding boxes of the five computational windows (Fig. 1) and the number of Argo probe cycles within each window within the depth range from 800 m to 1400 m.

Window	Longitude	Latitude	Number of Probe Cycles
A	28°–43° W	30°–42° N	4174
B	30°–50° W	20°–38° N	13716
C	39°–55° W	08°–28° N	11133
D	20°–49° W	0°–16° N	13320
E	20°–46° W	4° S - 08° N	8161

southwest Pacific (Yearsley and Sigwart, 2011). Distributions of probe headings were similar across the five computational windows (Fig. 3), although window E (straddling the equator) had an excess of probe displacements towards the west. The Argo probe data were used to estimate ocean current vector fields for each computational window on a 0.1° longitude-latitude grid, following the approach of (Yearsley and Sigwart, 2011). The estimated current vector fields are averaged over all 14 years of Argo probe data in order to maximise the spatial density of the data. Although the temporal variability is predicted to add some structure when temporal averaging is kept below two years (see Supplementary Material), there is little change in temporal structure when averaging across more than two years. In comparison, spatial averaging strongly reduces the structure in the estimated currents. This suggests that simulations should favour a fine spatial resolution at the expense of temporal resolution. For each computational window, 500 vector fields were generated.

There are several examples of using Argo probes to estimate deep-ocean currents (e.g Lebedev et al., 2007; Park et al., 2005; Roiha et al., 2018). The principal error using this approach comes from the influence of relatively strong surface currents upon the displacement of an Argo probe. This error is greatest when the direction of surface currents and deep currents are correlated. Following a similar method to Lebedev et al. (2007), and based on a probe descent and ascent rate of roughly 8 cm/s, a surface current five times faster than at depth and a linear relationship of current speed with depth (Lebedev et al., 2007; Roiha et al., 2018) gives a worst-case error estimate of 10% on ocean currents at 1000 m.

2.3. Release points

Fifty-four vent sites (active and inactive) from the InterRidge database (Version 3.4, https://vents-data.interridge.org/) are located within the five computational windows and used in the simulations. The spacing of vents on the nMAR is predicted to be on the order of 1 vent per 100 km (Beaulieu et al., 2015), so in addition to the 54 known vent sites, we added 34 'phantom' vent sites evenly spaced along sections of the nMAR where no vent sites have yet been detected (Fig. 1). Such 'phantom' vents have also been inferred from the discrepancy between dispersal capacity of mussels based on an ocean circulation model and contemporary migration rates of mussels based on genetic markers (Breusing et al., 2016).

2.4. Larval particle simulations

We simulated the release of over 10 million larval particles in the vicinity of 88 vent sites (either actual or phantom vent sites) along the nMAR (Fig. 1). These simulations were split into five computational windows (Table 1, Fig. 1) in order to reduce the memory requirements without limiting the particle simulations. The release positions of larval particles at each vent site were drawn from a 2-dimensional normal distribution, centred at the vent site, with a standard deviation of 0.05°.

Larval dispersal was simulated by estimating the movements of free-floating neutrally buoyant particles driven by Argo probe ocean current vector fields; see Yearsley and Sigwart (2011) for details of the methodology. Larval dispersal was simulated for up to 500 d for larval particles that stayed within a computational window. All simulations were performed in MATLAB version 2017b (Mathworks, 2017).

To ensure our final analyses were based upon a uniform spread of release locations along the nMAR, we defined 64 non-overlapping target boxes (each a 0.4° square box) that contained the 88 release points (Fig. 1). All our connectivity analyses used a randomly selected set of 6.4 million larval particles, comprising 10^5 simulated larval particles from

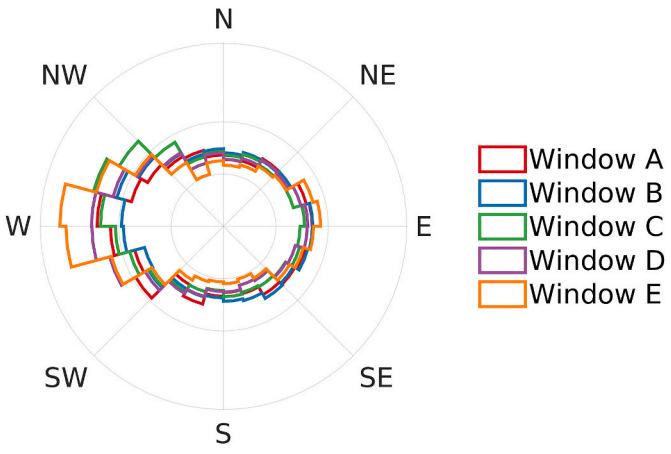

Fig. 3. The distribution of probe headings from probes at 800-1400 m depth for the five computational windows. The distance of each colored line from the origin represents the probability density of probes traveling along a range of bearings.

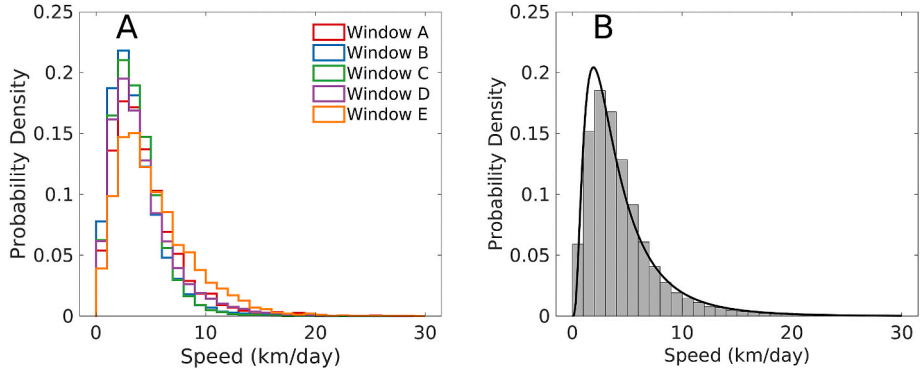

Fig. 2. A) Distribution of estimated probe speeds at 800-1400 m depth for the five computational windows (A-E). B) Combined distribution of probe speeds (bars) and the fitted Gamma distribution (solid line). The Gamma distribution has a shape parameter of 2.04 [95% CI: 2.02-2.07] and a scale parameter of 2.18 [95% CI: 2.16-2.21], giving a median probe speed of 3.8 km/day (equivalent to 4.3 cm/s) with 25% and 75% quartiles of 2.2 km/day and 6.0 km/day, respectively.

each target box.

Dispersal kernels for larval particles from each computational window were calculated using a normal kernel with a bandwidth of 20 km and dispersal distances calculated as great circle distances.

2.5. Connectivity

Connectivity time was estimated among the 64 target boxes along the nMAR. This connectivity time is an estimate of potential connectivity, assuming passive larval particles and mortality as a threshold PLD. For each target box we randomly picked 10^5 larval particles that had a release location within the target box. The connectivity time from target box i to target box j, $T_{i\to j}$, for each of the 10^5 larval particles released inside target box i was estimated as the number of days taken before the larval particle travelled through target box j. We set $T_{i\to j}$ to infinity if a larval particle did not travel through target box j within the maximum simulation time (500 days). The probability of connection from target box i to target box j within a maximum time t_{max}, $P(i\to j, t_{max})$, can then be estimated as the proportion of particles from target box i with $T_{i\to j} \leq t_{max}$.

A connectivity dendrogram for the connectivity times between target boxes was generated by setting a critical connection probability of $P_{crit} = 10^{-4}$ and calculating the minimum t_{max} that would give $P(i\to j, t_{max}) > P_{crit}$ or $P(j\to i, t_{max}) > P_{crit}$ (Fig. 5). This connectivity dendrogram visualises clusters of target boxes (connectivity regions) that can be connected (sometimes after multiple dispersal steps) above the critical connection probability within a maximum PLD.

The connectivity dendrogram contains no information about the north-south asymmetry in connectivity along the nMAR. To quantify the asymmetry in the source of connectivity for target box i we calculated the number of target boxes to the north of i, N_{north} (and similarly to the south of i, N_{south}) that achieved a connection probability $P(j\to i, t_{max} = 75$ days$) > 10^{-4}$. We then calculated an asymmetry index N_{north} - N_{south}. If connectivity is predominantly due to particles from the south then this index is negative. An index of zero indicates no north-south asymmetry in the source location of connecting larval particles.

3. Results

3.1. Dispersal distance and speed

Using estimated mid-water (1000 m) currents to drive simulated larval dispersal, we find that the median dispersal distance reaches 100 km (a typical distance scale between hydrothermal vent-sites) for PLDs of roughly 75 d (Table 2). The straight-line speed of these simulated larvae (1.3 km d^{-1}, Table A.1, Fig. A.3) is approximately three times slower than the median speed of Argo probes, 3.8 km d^{-1} (Fig. 2), due to the tortuosity of the path of the simulated larva. Median straight-line dispersal speed also declines within increasing PLD (Fig. A.1 & A.2, Table A.1 & A.2), with speeds approximately scaling with $PLD^{-0.25}$, although this scaling varies along the length of the nMAR (Table A.2). In the center of our study region, dispersal speeds are slowest and show little decline with increasing PLD. Dispersal speeds are highest at the extreme north (window A) and south (window E) of our study region, and also show a pronounced decline with increasing PLD. The distribution of straight-line dispersal distances shows right-skew (evidence of long-distance dispersers) PLDs of 75 to 100 d (Fig. 4, Table 2).

Table 2
The quantiles of dispersal distances across all simulated larval particles after 25, 50, 75, 100, 200 and 300 days of dispersal.

Dispersal	Quantiles of dispersal distance (km)				
Interval	5%	25%	50%	75%	95%
25 days	10	23	39	63	122
50 days	18	43	71	109	230
75 days	23	58	99	159	321
100 days	26	70	123	205	393
200 days	36	102	195	316	625
300 days	43	127	252	407	802

3.2. Regions of connectivity along the nMAR

Connectivity occurs between neighboring target boxes along the nMAR for realistic values of PLD, despite a tendency for simulated larvae to drift westwards, off the main axis of the nMAR (Fig. A.1 & A.2). Setting a maximum PLD of 75 d and a critical connection probability of 10^{-4}, the target boxes along the nMAR (Fig. 1) clustered into eight connected regions (Fig. 5). This implies that large parts of the nMAR could be connected, albeit after several generations of dispersal. Increasing the maximum PLD increases connectivity and reduces the number of connected regions (Fig. 5 & A.4). However, PLDs greater than 100 d have little effect on connectivity. For a PLD from 100 to 290 d and a critical connection probability of 10^{-4}, there are persistent barriers to

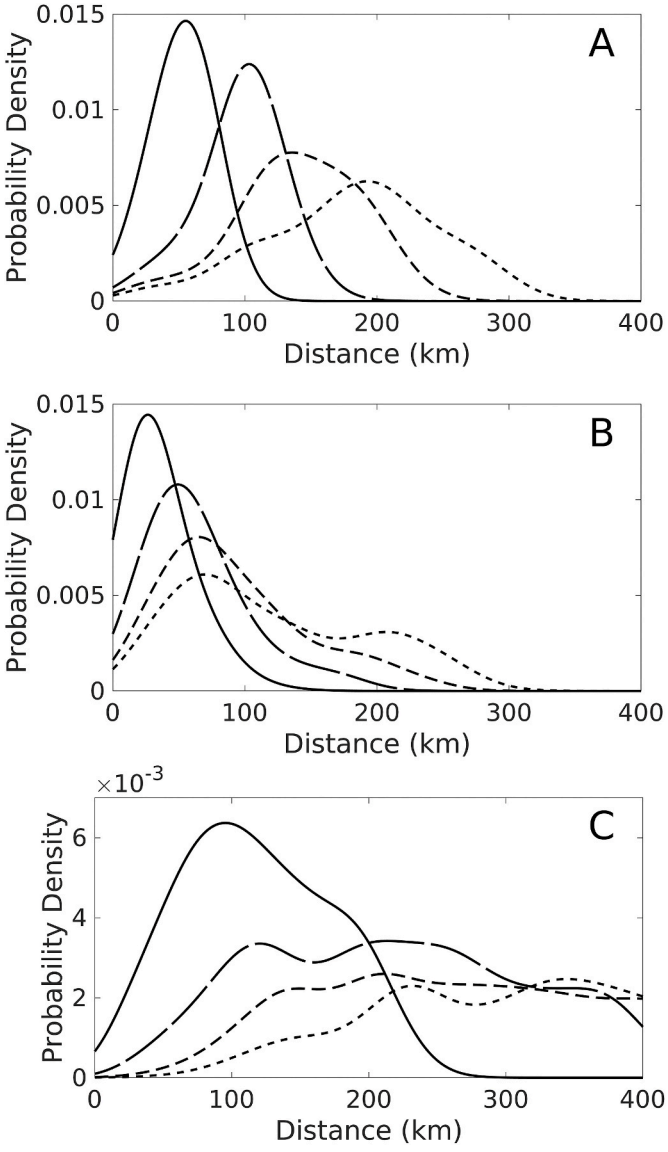

Fig. 4. A-C) Dispersal kernels for all simulated particles within computational windows A, C, E. Inset: Locations of computational windows. The dispersal kernels show the distribution of distances after dispersal after 25 d (solid line), 50 d (long dashed line), 75 d (medium dashed line), 100 d (short dashed line). A Gaussian smoother with a bandwidth of 20 km was applied to dispersal kernels.

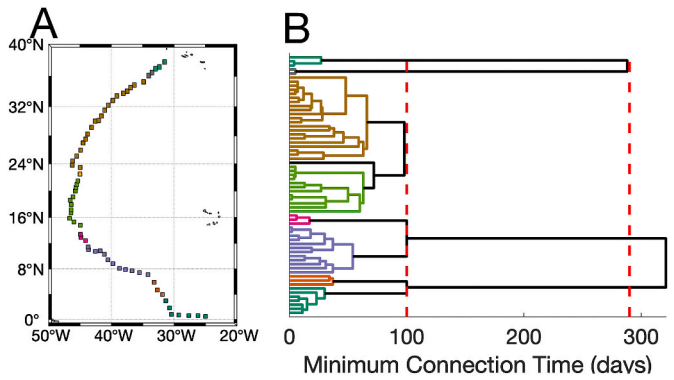

Fig. 5. A) Connectivity dendrogram for the minimum connection time that gives a probability of connectivity between two boxes greater than 10-4. The leaves of the dendrogram correspond to the 64 boxes shown in the map. B) Connected regions for a minimum connection time of 75 days are represented by the colours in the dendrogram and the colours of the boxes on the map. Vertical red dashed lines mark PLDs of 100 d and 290 d.

connectivity at about 6°N, 15°N, 36°N and 37°N.

3.3. Asymmetry in connectivity along the nMAR

Simulated connectivity along the nMAR shows a changing north-south asymmetry (Fig. 6). Simulated larval dispersal shows a strong westerly drift at the southern extent of the study region. This westerly drift combined with the curvature of the nMAR facilitates connectivity of larvae from the south with more northerly target boxes (Fig. 6). Persistent barriers to connectivity commonly correspond to sections of the nMAR where the connectivity asymmetry shows a strong change of direction. These strong changes in asymmetry can sometimes be seen as regions of easterly drift that counters the generally westerly drift of simulated larvae (Fig. A.1 & A.2).

4. Discussion

Larval dispersal potential in mid-water (1000 m) varies along the nMAR in the Argo model simulation, with the strongest directional (westerly) component near the equator. In this equatorial region, dispersal kernels include extended tails with long-distance dispersal potential (250 to 400 km or more, depending on PLD). This finding is consistent with strong mean zonal currents at 1000 m depth in the equatorial (0–6°N, Fig. 1) north Atlantic that, depending on the time of year, oscillate between east and west (Ollitrault and Colin de Verdière, 2013; Colin de Verdière and Ollitrault, 2016). Zonal flows tend to carry larvae away from the axis of the nMAR. Thus, while dispersal distances could be considerable in the equatorial Atlantic, larvae with long PLDs will not contribute to connectivity of vent sites along the ridge axis in proportion to their numbers. Strong equatorial zonal flows in the interior of the Atlantic Ocean may serve as an isolating filter for mussel larvae with long PLDs [90–120 d; (Colaço et al., 2006)], as observed in differences in mussel (*Bathymodiolus* spp.) lineages across the equator (Breusing et al., 2016; van der Heijden et al., 2012). Populations of vesicomyid clams (*Abyssogena southwardae*) and rimicarid shrimp (*Rimicaris exoculate*) occur at vents both north and south of the equator, however, suggesting that the equatorial region is not a barrier to their dispersal (Teixeira et al., 2012; van der Heijden et al., 2012). But *A. southwardae* occurs at seeps as well as vents (i.e., it has source populations off-axis), and coalescent methods detected gene flow between Barbados seeps and vent sites on the northern and southern Mid-Atlantic Ridge (LaBella et al., 2017), obviating a need to cross any equatorial barrier. And, unlike the sedentary adults and weakly swimming veliger larvae mussels and clams, *R. exoculata* is a robust swimmer as an adult and even during its post-larval stage; it and other vent shrimp taxa may not fit a passive-drifter model for dispersal (Teixeira et al., 2013).

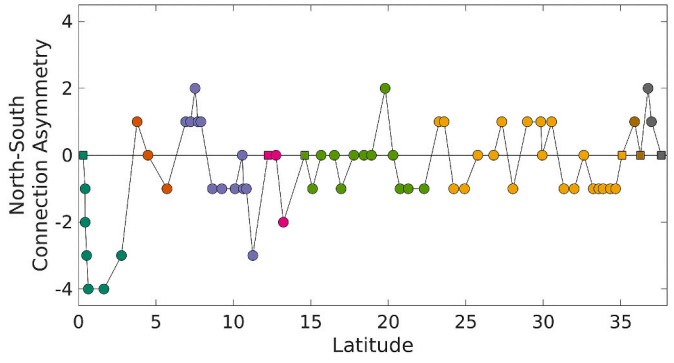

Fig. 6. The north-south asymmetry in the source location of particles received at the 64 target boxes along the nMAR. Negative/positive values indicate received particles predominantly from the south/north. Asymmetries are calculated based upon a minimum connection probability of 10-4 and a maximum planktonic larval duration of 75 days. Colours correspond to the colours for connectivity regions in figure 5. Square markers indicate target boxes that received no particles within 75 days.

Median dispersal distances were 100 km or less in the northern-most computational window for PLDs of 100 d or less. This is roughly in agreement with an independent biophysical model developed for the northern edge of window A and into the EEZ surrounding the Azores, where median dispersal distances did not exceed 150 km for PLDs of 180 d [Breusing et al., 2016; Viking 20 ocean general circulation model, with probability distributions summed through the entire water column].

A PLD of 70 d has been suggested as representative of 75% of deep-sea invertebrate species for which PLD has been estimated, based on life-history studies of a limited number of taxa (Hilário et al., 2015). Elsewhere, temperature- (and hence depth-) dependent PLDs of between 40 d (500 m depths) and 85 d (1000 m depths) have been used as average PLDs of deep-sea taxa (Mitarai et al., 2016). Median dispersal distances for a 70-d PLD were on the order of 140 km in the northern and 300 km in the southern region of the Argo-based model (Table 3). The 75th percentile dispersal distance for a subset of (mostly Pacific) vent invertebrates (n = 8 taxa) using genetic data has been estimated to be on the order of 100 km (Baco et al., 2016). Spatial scales of dispersal estimated from genetic data (Baco et al., 2016) and from two different types of biophysical models (Mitarai et al., 2016; this study) thus contribute to the weight of evidence bracketing median dispersal distances for non-swimming larvae at 25 to 200 km on the nMAR, depending on PLD (from 25-d to 100-d) and point of release. This corresponds to dispersal speeds of 1 to 2 km d^{-1}, which are within the range estimated for deep-sea larvae elsewhere (Table 4).

The connectivity dendrogram (Fig. 5B) suggests the potential for numerous relatively closed systems for taxa with short PLDs (i.e., little genetic connectivity between target regions). Fewer, larger zones of connectivity (>20 degrees of latitude or >2000 km) are suggested for

Table 3
The median dispersal distance (km) across all simulated larval particles in each computational window (A-E, Fig. 1) after 25, 50, 75, 100, 200 and 300 days of dispersal.

Dispersal	Computational Window				
Interval	A	B	C	D	E
25 days	55	31	28	44	113
50 days	100	51	55	82	216
75 days	142	67	79	110	304
100 days	187	79	105	130	377
200 days	261	100	213	177	585
300 days	300	114	313	209	741

Table 4
Estimated dispersal speeds for non-swimming deep-sea larvae and current speeds near the seabed in an axial valley of the nMAR derived from ocean general circulation models or Eulerian velocity fields from speeds and headings of the Argo fleet.

Geographic Region	Speeds (depth)	Reference
Estimated dispersal speeds from models and velocity fields		
NW Atlantic	1 (2500–3200 m) to 2 (1500–2000 m) km d^{-1}	Etter and Bower (2015)
NW Atlantic and Gulf of Mexico	1 (500 m) to 6 (100 m) km d^{-1}	Young et al. (2012)
Tropical S Pacific	1 (1440 m) to 4 (800 m) km d^{-1}	Yearsley and Sigwart (2011)
NE Atlantic	0.5 (600–2000 m) km d^{-1}	(Sala et al., 2013)
N Mid-Atlantic Ridge	1 to 2 km d^{-1} (1000 m)	*This study*
Current speeds measured in the field		
N MAR Axial Valley (FAMOUS Segment)	2.5 to 6.9 km d^{-1} (near bottom, within the axial valley)	Keller et al. (1975)

taxa with long PLDs up to 100 d, consistent with dispersal distance generally scaling with PLD (Shanks et al., 2003). However, for PLDs of 100 d and more, the scaling of connectivity with PLD is suspended, suggesting the existence of four persistent, mid-water hydrographic barriers to dispersal under the conditions of the velocity field derived from Argo float displacements. These mid-water hydrographic barriers for PLDs of ≥100 d are not aligned with major mid-water zonal flows at the same depth (Ollitrault and Colin de Verdière, 2013; Colin de Verdière and Ollitrault, 2016), except perhaps the easterly flow in the 5°N region (Fig. 1). The barriers 36° and 37° N (towards the north of our computational windows) are in a region where the bathymetry starts to become increasingly less than 1000 m as nMAR rises towards the Azores. Hence, the topography of the seabed is likely influencing the trajectories of Argo probes in this region and could explain the estimated persistent barrier. Large off-set fracture zones have been hypothesized as barriers to larval dispersal (Van Dover et al., 2002), but only one of the nine major nMAR transform faults [Oceanographer FZ at ~35°N, with >100 km offsets (Müller and Roest, 1992)] was associated with a mid-water hydrographic barrier to gene flow here. The modelled barrier suggests that taxa with mid-water PLDs of 100 d or more do not always increase connectivity among populations in a region. Our estimates of connectivity do not include larval behavior and therefore provide estimates of the bounds of dispersal ranges (Hilário et al., 2015). Including larval behavior in connectivity estimates will require a better understand of life-history for deep-sea species (Hilário et al., 2015) as well as a vertically resolved hydrodynamic model, since shallow water simulations show that vertical swimming behavior can affect connectivity estimates (e.g. North et al., 2008). Our simulations treat mortality as a threshold PLD. Additional mortality processes, such as a constant mortality rate, will primarily weaken the probability long-range dispersal and increase the probability of connectivity barriers. Any mortality process that is only a function of time (e.g. independent of a larval particle's local environmental, such as a constant mortality) will rescale the time axis of Fig. 5, but the topology of the dendrogram in Fig. 5 will be unaltered.

Despite model evidence for persistent mid-water biophysical barriers for taxa with long PLDs, to date there is no evidence for population structure correlated with these barriers. Current genetic markers may lack sufficient resolution to work well within (rather than across) species (Breusing et al., 2016), or sample sizes used for genetic studies have not been of sufficient size to have the statistical power to detect population structure (Collins et al., 2013a, 2013b). Barriers to connectivity might lead to opportunities for hybridization. Intriguingly, the mussel hybrid zone for *Bathymodiolus azoricus* and *B. puteoserpentis* at Broken Spur (Won et al., 2003; O'Mullan et al., 2001) is located at a break in mid-water hydrographic connectivity for PLDs up to 65 d (median dispersal distance on the order of 80 km), though without further weight of evidence, this could simply be coincidence.

Our predictions of larval dispersal and population connectivity are based upon one depth layer (800–1400 m) that is unlikely to be affected by topographic features, and on a coarse spatial resolution of hydrography that does not resolve sub-mesoscale oceanographic features (McWilliams, 2016). The implication of these conditions upon our results is unclear. Based on Vic et al.'s (2018) detailed oceanographic study for the Lucky Strike hydrothermal vent site, the effect of depth upon larval dispersal is scale dependent. Relative horizontal dispersion for pairs of particles increases with depth on time scales less than 10 d (moving from 600 m to 1800 m increases particle dispersion over 10 d by roughly 30 km) and decreases with depth on timescales of 100 d (moving from 600 m to 1800 m decreases particle dispersion over 100 d by roughly 100 km). Larvae that disperse near the seabed rather than mid-water will encounter hydrographic conditions complicated by strong interactions with topography, especially along the ridge axis. Including sub-mesoscale features into simulations does not change absolute dispersion, but increases the relative diffusivity of particle clouds (Vic et al., 2018). One effect of this increased diffusivity could be to weaken oceanographic barriers to connectivity.

While arguments have been put forward calling for protection of all active hydrothermal vent ecosystems from habitat destruction from extraction of polymetallic sulfides (Van Dover et al., 2018), such protection, if applied, would protect only the benthic life-history stage of vent organisms. There is also a need to protect the pelagic habitat of the dispersive larval stages that are essential for maintenance of the fragmented benthic populations. The model and approaches presented here could guide future sampling of planktonic larvae that could be checked for presence of hydrothermal-vent endemic species using traditional morphological methods or using species-specific genetic approaches to further describe the pelagic distribution of these organisms. For taxa with mid-water dispersing larvae (i.e., not in the axial valley for some portion of their PLD), a minimum requirement would be to protect areas within each of the connectivity regions identified in the 100 d PLD models for the nMAR. These areas would need to be large enough (i.e., on the order of 200 km along the ridge axis and 200 km across the ridge axis in the southern portion of the nMAR) to allow for protection of larvae with both short and long dispersal distances. Replication of these areas within connectivity zones should be maximized. The extent to which these dimensions are appropriate for near-bottom larval dwellers is unclear, but given measured current speeds in the axial valley in excess of estimated dispersal speeds (Table 3), protecting mid-water dispersal potential may prove to be a precautionary approach. The design parameters identified here (connectivity regions, dispersal potentials) can inform strategies for design of networks of no-mine areas distributed latitudinally along the nMAR (Dunn et al., 2018). An important next step will be to apply ocean general circulation models for the nMAR region to test how generalizable the mid-water (1000 m) Argo velocity fields may be and to undertake Lagrangian particle simulations within and above the axial valley for realistic scenarios that encompass a range of larval behaviors.

5. Conclusions

Mid-water larval dispersal ability as modelled here is generally predicted to transport larvae over distances of 100 km for a PLD of 75 d. However, the design of a network of deep-sea no-mine areas should take into account the spatial variation in dispersal ability along the nMAR. We identify two types of spatial variation: variation on the spatial scale of dispersal, with the weakest dispersal in the center of our region; and persistent barriers to dispersal at discrete points along the nMAR that can prevent connectivity even for very long PLDs. Results such as these can be applied globally to the mid-ocean ridge system to inform the design of no-mine areas (dimension and location) to protect the larval phase of benthic invertebrate life histories.

Research data

The Argo data were collected and made freely available by the International Argo Program and the national programs that contribute it. (http://www.argo.ucsd.edu, http://argo.jcommops.org). The Argo Program is part of the Global Ocean Observing System. http://doi.org/10.17882/42182 [accessed February 2017]. Locations of known vent sites were downloaded from InterRidge Vent Database (Version 3.4, https://vents-data.interridge.org/) [accessed March 2017]. Bathymetry uses ETOPO1 data from NOAA (Amante and Eakins, 2009) [accessed February 2017].

Connectivity, Argo probe, simulated larval tracks and vent data from this manuscript are available at DOI: http://doi.org/10.5281/zenodo.3525233.

CRediT authorship contribution statement

J.M. Yearsley: Conceptualization, Data curation, Formal analysis, Project administration, Software, Supervision, Validation, Visualization, Writing - original draft, Writing - review & editing. **D.M. Salmanidou:** Formal analysis, Software, Validation, Visualization, Data curation. **J. Carlsson:** Writing - review & editing. **D. Burns:** Software, Data curation. **C.L. Van Dover:** Conceptualization, Project administration, Writing - original draft, Writing - review & editing, Funding acquisition.

Declaration of competing interest

The authors declare that they have no known competing financial interests or personal relationships that could have appeared to influence the work reported in this paper.

Acknowledgements

This project was supported by the Global Ocean Biodiversity Initiative through the International Climate Initiative (IKI; grant number 16_IV_049_Global_A_Global Ocean Biodiversity Initiative GOBI). The Federal Ministry for the Environment, Nature Conservation, and Nuclear Safety (BMU) supports IKI on the basis of a decision adopted by the German Bundestag.

Appendix A. Supplementary data

Supplementary data to this article can be found online at https://doi.org/10.1016/j.dsr2.2020.104819.

References

Adams, D.K., Arellano, S.M., Govenar, B., 2012. Larval dispersal: vent life in the water column. Oceanography 25, 256–268. https://doi.org/10.5670/oceanog.2012.24.

Amante, C., Eakins, B.W., 2009. ETOPO1 1 Arc-Minute Global Relief Model: Procedures, Data Sources and Analysis. NOAA Technical Memorandum NESDIS NGDC-24. https://doi.org/10.7289/V5C8276M.

Baco, A.R., Etter, R.J., Ribeiro, P.A., von der Heyden, S., Beerli, P., Kinlan, B.P., 2016. A synthesis of genetic connectivity in deep-sea fauna and implications for marine reserve design. Mol. Ecol. 25, 3276–3298. https://doi.org/10.1111/mec.13689.

Beaulieu, S.E., Baker, E.T., German, C.R., 2015. Where are the undiscovered hydrothermal vents on oceanic spreading ridges? Deep Sea Res. Part II Top. Stud. Oceanogr. 121, 1–11. https://doi.org/10.1016/j.dsr2.2015.05.001.

Breusing, C., Biastoch, A., Drews, A., Metaxas, A., Jollivet, D., Vrijenhoek, R.C., Bayer, T., Melzner, F., Sayavedra, L., Petersen, J.M., Dubilier, N., Schilhabel, M.B., Rosenstiel, P., Reusch, T.B.H., 2016. Biophysical and population genetic models predict the presence of "phantom" stepping stones connecting Mid-Atlantic Ridge vent ecosystems. Curr. Biol. 26, 2257–2267. https://doi.org/10.1016/j.cub.2016.06.062.

Brooke, S.D., Young, C.M., 2009. Where do the embryos of *Riftia pachyptila* develop? Pressure tolerances, temperature tolerances, and buoyancy during prolonged embryonic dispersal. Deep-Sea Res. Part II Top. Stud. Oceanogr. 56, 1599–1606. https://doi.org/10.1016/j.dsr2.2009.05.003.

Colaço, A., Martins, I., Laranjo, M., Pires, L., Leal, C., Prieto, C., Costa, V., Lopes, H., Rosa, D., Dando, P.R., Serrão-Santos, R., 2006. Annual spawning of the hydrothermal vent mussel *Bathymodiolus azoricus* under controlled aquarium, conditions at atmospheric pressure. J. Exp. Mar. Biol. Ecol. 333, 166–171. https://doi.org/10.1016/j.jembe.2005.12.005.

Colin de Verdière, A.C., Ollitrault, M., 2016. A direct determination of the World Ocean barotropic circulation. J. Phys. Oceanogr. 46, 255–273. https://doi.org/10.1175/JPO-D-15-0046.1.

Collins, P.C., Croot, P., Carlsson, J., Colaço, A., Grehan, A., Hyeong, K., Kennedy, R., Mohn, C., Smith, S., Yamamoto, H., Rowden, A., 2013a. A primer for the Environmental Impact Assessment of mining at seafloor massive sulfide deposits. Mar. Pol. 42, 198–209. https://doi.org/10.1016/J.MARPOL.2013.01.020.

Collins, P.C., Kennedy, B., Copley, J., Boschen, R., Fleming, N., Forde, J., Ju, S.-J., Lindsay, D., Marsh, L., Nye, V., Patterson, A., Watanabe, H., Yamamoto, H., Carlsson, J., David Thaler, A., 2013b. VentBase: developing a consensus among stakeholders in the deep-sea regarding environmental impact assessment for deep-sea mining–A workshop report. Mar. Pol. 42, 334–336. https://doi.org/10.1016/J.MARPOL.2013.03.002.

Cowen, R.K., Sponaugle, S., 2009. Larval dispersal and marine population connectivity. Annu. Rev. Mar. Sci. 1, 443–466. https://doi.org/10.1146/annurev.marine.010908.163757.

Danabasoglu, G., Yeager, S.G., Bailey, D., Behrens, E., Bentsen, M., Bi, D., Biastoch, A., Böning, C., Bozec, A., Canuto, V.M., Cassou, C., Chassignet, E., Coward, A.C., Danilov, S., Diansky, N., Drange, H., Farneti, R., Fernandez, E., Fogli, P.G., Forget, G., Fujii, Y., Griffies, S.M., Gusev, A., Heimbach, P., Howard, A., Jung, T., Kelley, M., Large, W.G., Leboissetier, A., Lu, J., Madec, G., Marsland, S.J., Masina, S., Navarra, A., George Nurser, A.J., Pirani, A., y Mélia, D.S., Samuels, B.L., Scheinert, M., Sidorenko, D., Treguier, A.M., Tsujino, H., Uotila, P., Valcke, S., Voldoire, A., Wang, Q., 2014. North Atlantic simulations in coordinated ocean-ice reference experiments phase II (CORE-II). Part I: mean states. Ocean Model. 73, 76–107. https://doi.org/10.1016/j.ocemod.2013.10.005.

Dunn, D.C., Van Dover, C.L., Etter, R.J., Smith, C.R., Levin, L.A., Morato, T., Colaço, A., Dale, A.C., Gebruk, A.V., Gjerde, K.M., Halpin, P.N., Howell, K.L., Johnson, D., Angel Perez, J.A., Chantal Ribeiro, M., Stuckas, H., Weaver, P., Workshop Participants, S., 2018. A strategy for the conservation of biodiversity on mid-ocean ridges from deep-sea mining. Sci. Adv. 1–16. https://doi.org/10.1126/sciadv.aar4313.

Etter, R.J., Bower, A.S., 2015. Dispersal and population connectivity in the deep North Atlantic estimated from physical transport processes. Deep Sea Res. Oceanogr. Res. Pap. 104, 159–172. https://doi.org/10.1016/j.dsr.2015.06.009.

Herring, P.J., Dixon, D.R., 1998. Extensive deep-sea dispersal of postlarval shrimp from a hydrothermal vent. Deep-Sea Res. Part I Oceanogr. Res. Pap. 45, 2105–2118. https://doi.org/10.1016/S0967-0637(98)00050-8.

Hilário, A., Metaxas, A., Gaudron, S.M., Howell, K.L., Mercier, A., Mestre, N.C., Ross, R.E., Thurnherr, A.M., Young, C., 2015. Estimating dispersal distance in the deep sea: challenges and applications to marine reserves. Front. Mar. Sci. 2, 1–14. https://doi.org/10.3389/fmars.2015.00006.

Jackson, L.C., Dubois, C., Forget, G., Haines, K., Harrison, M., Iovino, D., Köhl, A., Mignac, D., Masina, S., Peterson, K.A., Piecuch, C.G., Roberts, C.D., Robson, J., Storto, A., Toyoda, T., Valdivieso, M., Wilson, C., Wang, Y., Zuo, H., 2019. The mean state and variability of the North Atlantic circulation: a perspective from ocean reanalyses. J. Geophys. Res.: Oceans 124, 9141–9170. https://doi.org/10.1029/2019JC015210.

Keller, G.H., Anderson, S.H., Lavelle, J.W., 1975. Near-bottom currents in the Mid-Atlantic Ridge rift valley. Can. J. Earth Sci. 12, 703–710. https://doi.org/10.1139/e75-061.

Kim, S.L., Mullineaux, L.S., Helfrich, K.R., 1994. Larval dispersal via entrainment into hydrothermal vent plumes. J. Geophys. Res. 99, 12655. https://doi.org/10.1029/94JC00644.

LaBella, A.L., Van Dover, C.L., Jollivet, D., Cunningham, C.W., 2017. Gene flow between Atlantic and Pacific Ocean basins in three lineages of deep-sea clams (Bivalvia: Vesicomyidae: Pliocardiinae) and subsequent limited gene flow within the Atlantic. Deep-Sea Res. Part II Top. Stud. Oceanogr. 137, 307–317. https://doi.org/10.1016/j.dsr2.2016.08.013.

Lebedev, K.V., Yoshinari, H., Maximenko, N.A., Hacker, P.W., 2007. Yomaha'07: Velocity Data Assessed from Trajectories of Argo Floats at Parking Level and at the Sea Surface. International Pacific Research Center (IPRC) Technical Note.

Lodge, M., Johnson, D., LeGurun, G., Wengler, M., Weaver, P., Gunn, V., 2014. Seabed mining: international seabed authority environmental management plan for the Clarion–Clipperton zone. A partnership approach. Mar. Pol. 49, 66–72. https://doi.org/10.1016/j.marpol.2014.04.006.

Mathworks, 2017. MATLAB Version 9.3.0.713579 (R2017b). The Mathworks Inc., Natick Massachusetts.

McVeigh, D.M., Eggleston, D.B., Todd, A.C., Young, C.M., He, R., 2017. The influence of larval migration and dispersal depth on potential larval trajectories of a deep-sea bivalve. Deep-Sea Res. Part I Oceanogr. Res. Pap. 127, 57–64. https://doi.org/10.1016/j.dsr.2017.08.002.

McWilliams, J.C., 2016. Submesoscale currents in the ocean. Proc. Math. Phys. Eng. Sci. 472, 20160117. https://doi.org/10.1098/rspa.2016.0117.

Mitarai, S., Watanabe, H., Nakajima, Y., Shchepetkin, A.F., McWilliams, J.C., 2016. Quantifying dispersal from hydrothermal vent fields in the western Pacific Ocean. Proc. Natl. Acad. Sci. U.S.A. 113, 2976–2981. https://doi.org/10.1073/pnas.1518395113.

Müller, R.D., Roest, W.R., 1992. Fracture zones in the North Atlantic from combined Geosat and Seasat data. J. Geophys. Res. 97, 3337–3350. https://doi.org/10.1029/91JB02605.

Mullineaux, L.S., Metaxas, A., Beaulieu, S.E., Bright, M., Gollner, S., Grupe, B.M., Herrera, S., Kellner, J.B., Levin, L.A., Mitarai, S., Neubert, M.G., Thurnherr, A.M., Tunnicliffe, V., Watanabe, H.K., Won, Y.-J., 2018. Exploring the ecology of deep-sea

hydrothermal vents in a metacommunity framework. Front. Mar. Sci. 5, 1–27. https://doi.org/10.3389/fmars.2018.00049.
North, E.W., Schlag, Z., Hood, R.R., Li, M., Zhong, L., Gross, T., Kennedy, V.S., 2008. Vertical swimming behavior influences the dispersal of simulated oyster larvae in a coupled particle-tracking and hydrodynamic model of Chesapeake Bay. Mar. Ecol. Prog. Ser. 359, 99–115. https://doi.org/10.3354/meps07317.
Ollitrault, M., Colin de Verdière, A., 2013. The ocean general circulation near 1000-m depth. J. Phys. Oceanogr. 44, 384–409. https://doi.org/10.1175/jpo-d-13-030.1.
O'Mullan, G.D., Maas, P.A.Y., Lutz, R.A., Vrijenhoek, R.C., 2001. A hybrid zone between hydrothermal vent mussels (Bivalvia: Mytilidae) from the Mid-Atlantic Ridge. Mol. Ecol. 10, 2819–2831. https://doi.org/10.1046/j.0962-1083.2001.01401.x.
Palumbi, S.R., 2003. Population genetics, demographic connectivity, and the design of marine reserves. Ecol. Appl. 13, 146–158. https://doi.org/10.1890/1051-0761(2003)013[0146:PGDCAT]2.0.CO;2.
Park, J.J., Kim, K., King, B.A., Riser, S.C., Park, J.J., Kim, K., King, B.A., Riser, S.C., 2005. An advanced method to estimate deep currents from profiling floats. J. Atmos. Ocean. Technol. 22, 1294–1304. https://doi.org/10.1175/JTECH1748.1.
Ramirez Llodra, E., Tyler, P.A., Copley, J.T.P., 2000. Reproductive biology of three caridean shrimp, *Rimicaris exoculata, Chorocaris chacei* and *Mirocaris fortunata* (Caridea: Decapoda), from hydrothermal vents. J. Mar. Biol. Assoc. U. K. 80, 473–484. https://doi.org/10.1017/S0025315400002174.
Rittschof, D., Forward Jr., R., Cannon, G., Welch, J., Mcclary, M., Holm, E., Clare, A., Conova, S., Mckelvey, L., Bryan, P., Van Dover, C., 1998. Cues and context: larval responses to physical and chemical cues. Biofouling 12, 31–44. https://doi.org/10.1080/08927019809378344.
Roberts, C.M., 1997. Reefs connectivity and management of Caribbean coral reefs. Science 278, 1454–1457. https://doi.org/10.1126/science.278.5342.1454.
Roemmich, D., Johnson, G.C., Riser, S., Davis, R., Gilson, J., Owens, W.B., Garzoli, S.L., Schmid, C., Ignaszewski, M., 2009. The Argo program: observing the Global Ocean Argo program. Oceanography 22, 34–43. https://doi.org/10.5670/oceanog.2009.36.
Roiha, P., Siiriä, S.-M., Haavisto, N., Alenius, P., Westerlund, A., Purokoski, T., 2018. Estimating currents from Argo trajectories in the Bothnian Sea, Baltic Sea. Front. Mar. Sci. 5, 308. https://doi.org/10.3389/fmars.2018.00308.
Ross, R.E., Nimmo-Smith, W.A.M., Howell, K.L., 2016. Increasing the depth of current understanding: sensitivity testing of deep-sea larval dispersal models for ecologists. PloS One 11, 1–25. https://doi.org/10.1371/journal.pone.0161220.
Sala, I., Caldeira, R.M.A., Estrada-Allis, S.N., Froufe, E., Couvelard, X., 2013. Lagrangian transport pathways in the northeast Atlantic and their environmental impact. Limnol. Oceanogr. Fluids Environ. 3, 40–60. https://doi.org/10.1215/21573689-2152611.
Shanks, A.L., Grantham, B.A., Carr, M.H., 2003. Propagule dispersal distance and the size and spacing of marine reserves. Ecol. Appl. 13, 159–169. https://doi.org/10.1890/1051-0761(2003)013[0159:PDDATS]2.0.CO;2.
Teixeira, S., Olu, K., Decker, C., Cunha, R.L., Fuchs, S., Hourdez, S., Serrão, E.A., Arnaud-Haond, S., 2013. High connectivity across the fragmented chemosynthetic ecosystems of the deep Atlantic Equatorial Belt: efficient dispersal mechanisms or questionable endemism? Mol. Ecol. 22, 4663–4680. https://doi.org/10.1111/mec.12419.
Teixeira, S., Serrão, E.A., Arnaud-Haond, S., 2012. Panmixia in a fragmented and unstable environment: the hydrothermal shrimp *Rimicaris exoculata* disperses extensively along the Mid-Atlantic ridge. PloS One 7. https://doi.org/10.1371/journal.pone.0038521.
Thurnherr, A.M., Richards, K.J., German, C.R., Lane-Serff, G.F., Speer, K.G., 2002. Flow and mixing in the rift valley of the mid-Atlantic ridge. J. Phys. Oceanogr. 32, 1763–1778. https://doi.org/10.1175/1520-0485(2002)032<1763:famitr>2.0.co;2.
van der Heijden, K., Petersen, J.M., Dubilier, N., Borowski, C., 2012. Genetic connectivity between north and south Mid-Atlantic Ridge chemosynthetic bivalves and their symbionts. PloS One 7, e39994. https://doi.org/10.1371/journal.pone.0039994.
Van Dover, C., Arnaud-Haond, S., Gianni, M., Helmreich, S., Huber, J., Jaeckel, A., Metaxas, A., Pendleton, L., Petersen, S., Ramirez-Llodra, E., Steinberg, P., Tunnicliffe, V., Yamamoto, H., 2018. Scientific rationale and international obligations for protection of active hydrothermal vent ecosystems from deep-sea mining. Mar. Pol. 90, 20–28. https://doi.org/10.1016/j.marpol.2018.01.020.
Van Dover, C.L., German, C.R., Speer, K.G., Parson, L.M., Vrijenhoek, R.C., 2002. Evolution and biogeography of deep-sea vent and seep invertebrates. Science 295, 1253–1257. https://doi.org/10.1126/science.1067361.
Vic, C., Gula, J., Roullet, G., Pradillon, F., 2018. Dispersion of deep-sea hydrothermal vent effluents and larvae by submesoscale and tidal currents. Deep-Sea Res. Part I Oceanogr. Res. Pap. 133, 1–18. https://doi.org/10.1016/j.dsr.2018.01.001.
Vrijenhoek, R.C., 2010. Genetic diversity and connectivity of deep-sea hydrothermal vent metapopulations. Mol. Ecol. 19, 4391–4411. https://doi.org/10.1111/j.1365-294X.2010.04789.x.
Won, Y., Hallam, S.J., O'Mullan, G.D., Vrijenhoek, R.C., 2003. Cytonuclear disequilibrium in a hybrid zone involving deep-sea hydrothermal vent mussels of the genus *Bathymodiolus*. Mol. Ecol. 12, 3185–3190. https://doi.org/10.1046/j.1365-294X.2003.01974.x.
Yearsley, J.M., Sigwart, J.D., 2011. Larval transport modeling of deep-sea invertebrates can aid the search for undiscovered populations. PloS One 6, e23063. https://doi.org/10.1371/journal.pone.0023063.
Young, C.M., He, R., Emlet, R.B., Li, Y., Qian, H., Arellano, S.M., Van Gaest, A., Bennett, K.C., Wolf, M., Smart, T.I., Rice, M.E., 2012. Dispersal of deep-sea larvae from the Intra-American Seas: simulations of trajectories using ocean models. Integr. Comp. Biol. 52, 483–496. https://doi.org/10.1093/icb/ics090.